Banding Artifact Reduction in Electrophotographic Printers by Using Pulse Width Modulation

Guo-Yau Lin,▲ Jimmy M. Grice, and Jan P. Allebach,▲*
School of Electrical and Computer Engineering, Purdue University, West Lafayette, Indiana

George T.-C. Chiu▲
School of Mechanical Engineering, Purdue University, West Lafayette, Indiana

Wayne Bradburn and Jeff Weaver
Hewlett-Packard Company, Boise, Idaho

We propose a system to reduce electrophotographic laser printer banding artifacts due to optical photoconductor (OPC) drum velocity fluctuations. The drum velocity fluctuations are sensed with an optical encoder mounted on the drum axis. Based on the line-to-line differential encoder count, we modulate the laser pulse width to compensate fluctuations in development that would otherwise occur. We present an analysis of the system, including the compensation algorithm that determines the desired pulse-width as a function of differential encoder count. Characterization of the system is based on printing, scanning, and processing a special test page that yields information about line-spacing and absorptance fluctuations. This data is synchronized with the encoder count signal that was recorded during the printing of the test page. Finally, we present experimental results for an HP LaserJet 4M printer that demonstrate the effectiveness of the system in reducing banding due to OPC drum velocity fluctuations.

Journal of Imaging Science and Technology 46: 326–337 (2002)

Introduction

In this paper, we classify as *banding* those artifacts that are due to quasiperiodic fluctuations in process direction parameters. Since no variation in scan direction parameters is involved, the artifacts are constant in the scan direction. With laser printers, banding artifacts are primarily due to fluctuations in the angular velocity of the optical photoconductor (OPC) drum. These fluctuations result in non-uniform line spacing that causes a corresponding fluctuation in developed toner on the printed page.

Banding artifacts have been widely studied and modeled.[1–4] To reduce banding, one can either design a better mechanical system, or compensate the source of the banding through feedback. To improve the mechanical system, one can use larger diameter gears, which increases the frequencies associated with tooth-to-tooth fluctuations in drive train velocity. This will also increase the angular momentum of the system, which decreases the sensitivity to velocity disturbances. Alternatively, the gear train can be designed with a coupling mechanism to reduce velocity perturbations.[5] In a similar vein, design methods have been proposed to reduce banding induced by the charger roller[6] and cleaning blade.[7]

Feedback systems for banding compensation may be categorized into two groups. In the first group, we have systems that directly compensate the line spacing error via laser beam deflection.[8,9] In the second group, we have systems that indirectly compensate the line spacing error by varying the laser beam exposure.[10–13] Both types of systems require a sensor to detect the OPC drum angular velocity.

Among these banding reduction strategies, our work is most closely related to Morrison's invention,[12] which uses two interference gratings to obtain the OPC drum velocity, and proposes several means of adjusting the laser beam exposure or moving the laser diode. However, the system model and compensation scheme are not clearly discussed, nor are experimental results presented. In fact, few experimental results for any type of banding reduction strategy have been reported in the literature. In this paper, we present a system that uses laser beam pulse width modulation (PWM) to compensate fluctuations in line spacing. The line spacing information is obtained from an optical encoder mounted on the OPC axis. Our system is based on a 600 dpi HP LaserJet 4M printer (HP LJ4M: Hewlett-Packard Company, Boise, ID). All the

Original manuscript received October 17, 2001

▲ IS&T Member

*Corresponding Author: Jan P. Allebach, Phone: (765) 494-3535, Fax: (765) 494-3358

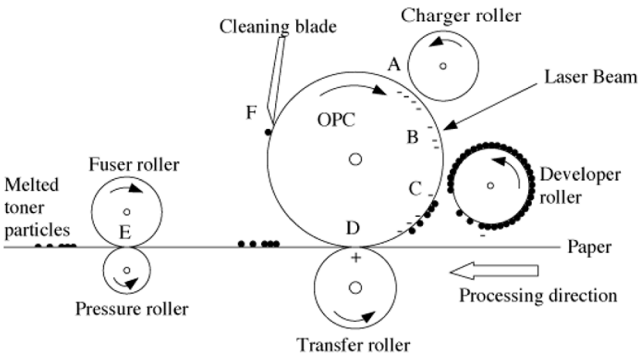

Figure 1. Electrophotographic process: cross-section of a typical laser printer (A) charging, (B) exposure, (C) development, (D) transferring, (E) fusing, and (F) cleaning.

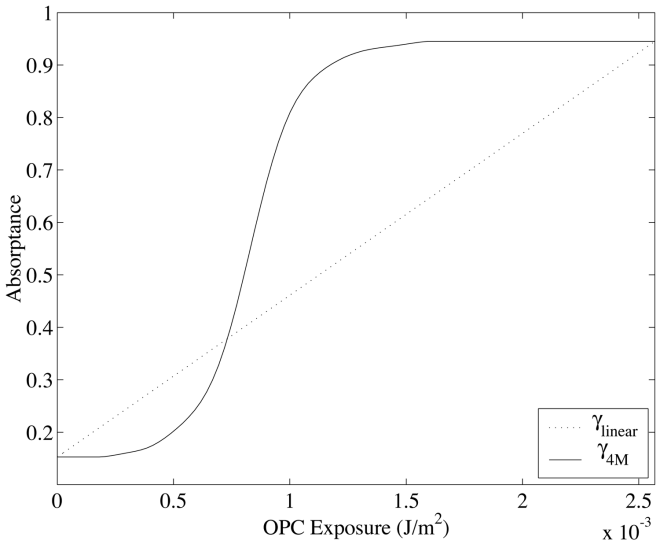

Figure 2. Mapping from energy exposure on the OPC to absorptance in the final print for the LaserJet 4M.

parameters and experimental results presented in this paper are for that printer. This paper is organized as follows. In the next section, we review the electrophotographic process, and show how it impacts banding. In the *Test Pattern Design and Analysis* section, we characterize the banding based on measurements from a printed test pattern. Section *Banding Reduction System* describes and analyzes the architecture of the system that we use to reduce banding. The compensation algorithm is derived from the established system models in the section *System Analysis*. We then present the experimental results, and finally, draw some conclusions from our work in the end of this article.

Electrophotographic Process and Banding

The Electrophotographic Process

The electrophotographic (EP) process[14–16] can be divided into six main steps, namely charging, exposure, development, transferring, fusing, and cleaning. Figure 1 shows these steps on the cross-section of a laser printer. First, the charger roller uniformly charges the OPC drum surface to a constant negative voltage. In the exposure step, the laser beam is scanned across the OPC and is turned on to discharge the OPC surface at appropriate locations. These discharged locations then attract the negatively charged toner particles in the development step. After development, the transfer roller applies a positive charge to the paper. This positive charge creates a force pulling the negatively charged toner particles to the paper. Next the paper passes between the heated fuser roller and a pressure roller which together melt the toner and fuse it to the paper. Finally, the non-transferred toner particles on the OPC drum are removed with the help of a blade or a brush.

To better understand the relation between the EP process and banding, it will be helpful to examine a model for the EP process. For this purpose, we consider the model developed in Ref. 17. First, the laser beam intensity is modeled as a 2-D Gaussian envelope

$$I(x,y) = I_0 \exp\left(-\frac{x^2}{2\sigma_x^2} - \frac{y^2}{2\sigma_y^2}\right) \quad \mathrm{W/m^2}, \quad (1)$$

where I_0 is the peak amplitude of the laser, and σ_x and σ_y are the beam widths in the scan and process directions, respectively. As the laser is scanned along the x direction, it is switched on and off. Let us assume that it is switched on at time 0 and off at time t_{off} and that its transitions obey an exponential model with rise time t_r and fall time t_f. The peak amplitude can then be expressed as

$$I_0(t) = \begin{cases} 0, & t < 0, \\ I_{\max}(1-\exp(-t/t_r)) & 0 \le t \le t_{off}, \\ I_{\max}(1-\exp(-t_{off}/t_r))(\exp(-(t-t_{off})/t_f)), & t > t_{off}. \end{cases} \quad (2)$$

Let us define d_x^0 and d_y^0 as the nominal values of the printed pixel width (in the scan direction) and height (in the process direction), respectively, and $(x(m), y(n))$ as the coordinates of the center of the (m, n)-th pixel. When the halftone pixel $g[m, n]$ is turned on, the laser beam is switched on at the physical coordinate $(x(m) - d_x^0/2, y(n))$ and off at $(x(m) + d_y^0/2; y(n))$. Let the laser beam be scanned at the speed V m/s, then $t_{off} = d_x^0/V$. Based on the 2-D laser beam Gaussian profile, the exposure of any arbitrary point (x, y) due to the halftone pixel $g[m, n]$ being printed is

$$E_{mn}(x,y) = \int_0^\infty I_0(t)\exp\left(-\frac{(x-(x(m)-d_x^0/2)-Vt)^2}{2\sigma_x^2} - \frac{(y-y(n))^2}{2\sigma_y^2}\right)dt \quad \mathrm{J/m^2}. \quad (3)$$

Since the contributions of each printed pixel to the total exposure on the OPC drum will be additive, we may write the total exposure as

$$E(x,y) = \sum_{\substack{m,n \\ g[m,n]=1}} E_{mn}(x,y). \quad (4)$$

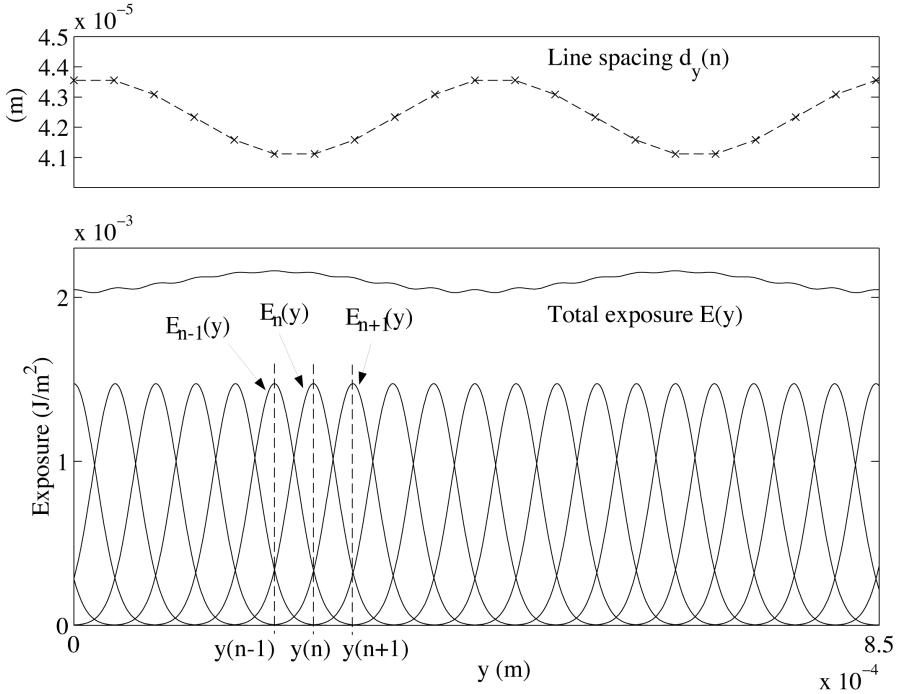

Figure 3. Banding simulation. Top: Scan line spacing. Bottom: Exposure $E_n(y)$ and total exposure $E(y)$ along the process direction for each column of pixels with value 1. For each scan line, the exposure has a Gaussian profile. Modulating the scan line spacing (60 cycles/in in this example) induces a corresponding modulation in the total exposure.

For the HP LaserJet 4M, $I_{\max} = 1.1$ mW/m^2, $d_x^0 = d_y^0 = 42.33$ μm, $V = 316$ m/s, $\sigma_x = 20.08$ μm (or 0.474 pixels) and $\sigma_y = 24.01$ μm (or 0.567 pixels).

The relation between exposure on the OPC, toner mass transferred during development, and final toner mass at any fixed position on the page after fusing is quite complex.[14–16] Following Kacker and co-workers,[17] we treat these two steps as a point-to-point nonlinear mapping γ from exposure E to absorptance a on the printed page. Figure 2 shows this relation γ_{4M} for the LaserJet 4M along with an ideal linear relationship γ_{linear} that would enable the device to render gray scale without halftoning. Our complete model for the EP process is then given by

$$a(x, y) = \gamma(E(x, y)). \tag{5}$$

The steep portion of the nonlinear curve for the actual printer will significantly enhance banding as we will see shortly.

Banding Artifacts

Let us now examine how fluctuations in line spacing produce banding. Suppose that the position $y(n)$ of the n-th scan line is perturbed by a single sinusoid with spatial frequency μ which has units of cycles/in. We can write

$$y(n) = y_0 + nd_y^0 + \delta_y \sin(2\pi n\mu d_y^0 + \psi_y), \tag{6}$$

where y_0 is the initial scan line position, and δ_y and ψ_y are respectively the amplitude and phase of the displacement perturbation. Combining Eqs. (2) through (6), we obtain the absorptance a of the printed image at any arbitrary point (x, y) for a given halftone image g.

To further examine the combined effect of the EP process and banding, we now consider the absorptance resulting from a given halftone image g. In order to simplify the result, we consider a uniform halftone pattern instead of a natural image. In particular, we consider a 50% fill pattern obtained by setting the pixels in the odd columns equal to 1 and the pixels in the even columns equal to 0.

As a numerical example, let $y_0 = 0$, $\psi_y = 0$, $\delta_y = 8 \times 10^{-5}$ in, and $\mu = 60$ cycles/in. Figure 3 shows the scan line spacing, the individual exposure profiles for each scan line, and the total exposure in the process direction. In this figure, the exposure curves represent the amplitude in the process direction for the columns of pixels that are turned on. From Fig. 3, we see that the total exposure along the process direction is modulated according to the frequency μ. This exposure modulation is then enhanced by the nonlinear mapping γ in the EP process. To observe this enhancement, we first map the total exposure to absorptance, and then project the absorptance on the y axis. Figure 4 shows the projected absorptance mapped by γ_{linear} and γ_{4M}. Comparing the effect of the linear mapping γ_{linear} with that corresponding to the actual printer γ_{4M}, we see how the banding is enhanced by the nonlinear relationship between exposure and absorptance.

Test Pattern Design and Analysis

To measure banding, we print a specially designed test page, then scan it, and analyze the scanned data. The test page is designed to show banding in the process direction and to also yield information about the scan line positions in the process direction.

Test Pattern Design

Figure 5 shows that the test pattern is separated into three vertical components. Along the left and right edges are a series of registration marks to establish the position of each scan line. These registration marks are stag-

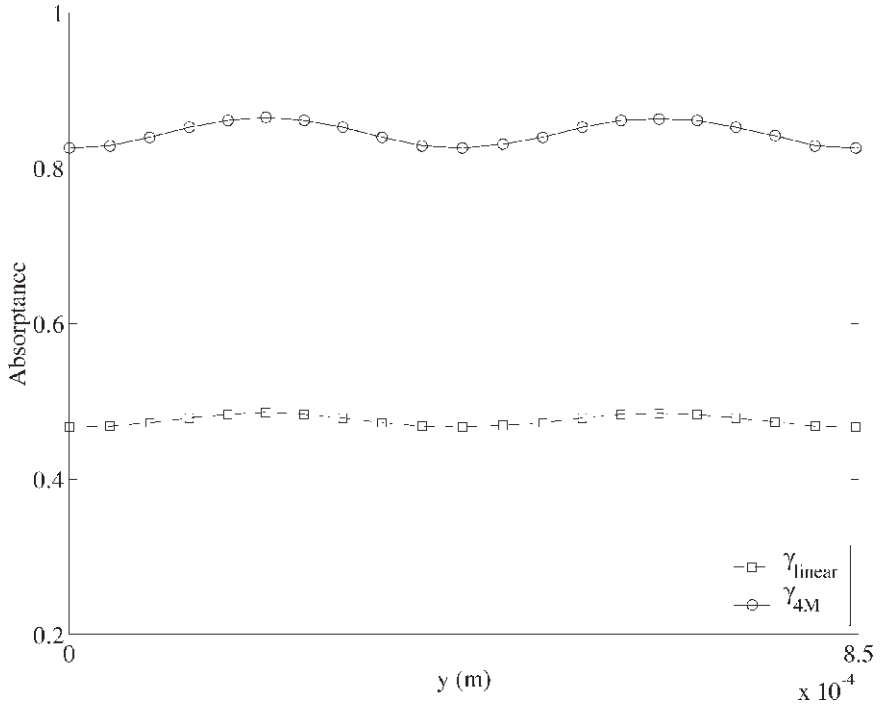

Figure 4. Projected absorptance of a simulated printed image in which a vertical line is printed at every other column of pixels. The simulated absorptance is mapped from total exposure with both an ideal linear transform and the actual nonlinear transform for the LaserJet 4M. The data points represent the locations of the scan lines.

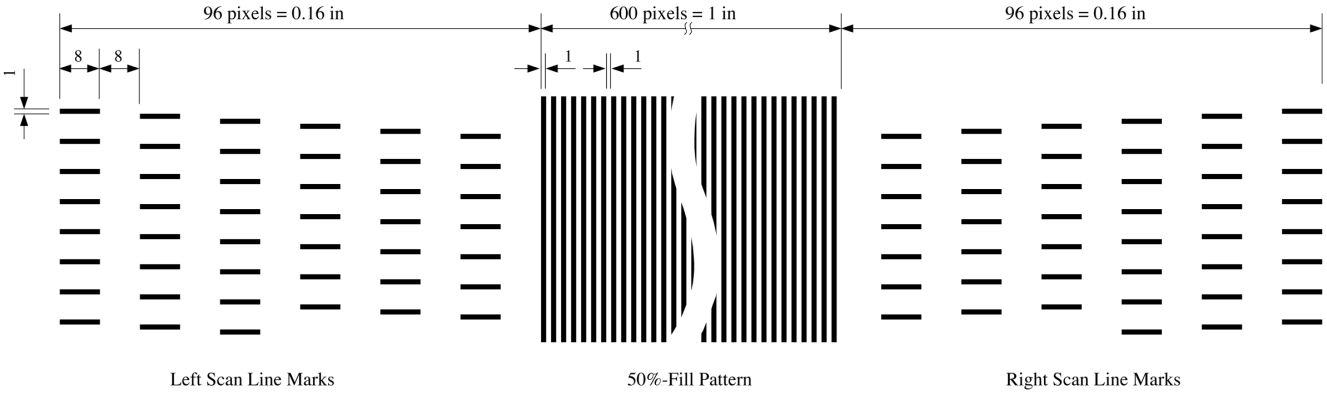

Figure 5. Layout of the test pattern. All units are in pixels unless shown otherwise. Banding is measured from the center 50% fill pattern. The registration marks on either side are used to determine scan line position.

gered from line-to-line to permit segmentation of the individual registration marks and to eliminate the interaction between the exposure of the marks on adjacent lines. Placing the marks symmetrically on either side of the page facilitates correction of skew due to misalignment of the printed page on the scanner drum.

The center region of the test pattern is used to measure the effect of the line spacing fluctuation on printed absorptance. Since banding is most apparent in flat midtone areas, we design a 50% fill test pattern as shown in Fig. 5 to measure it. In this 50% fill test pattern, we print a vertical line at every other column of addressable pixels. Compared with any other 50% fill pattern, this gives us the maximum spatial resolution of banding.

Test Pattern Analysis

After printing the test pattern, the next step is to extract the information from the print by scanning it on a high-resolution drum scanner (Howtek Scanmaster D4000: Howtek, Inc., Hudson, NH) at 2000 dpi. Figure 6 shows the scanned test pattern. First we segment the registration marks on the scanned image, and compute their centroids $y_L(n)$ and $y_R(n)$ along the process direction. We average these values to obtain our estimate $y(n) = {}^1/_2\,[y_L(n) + y_R(n)]$ of the position of the n-th line, and then compute the line spacing as $d_y(n) = y(n) - y(n-1)$.

With the help of the coordinates of the corresponding registration marks, we segment the scanned absorptance test pattern into cells indicated by the dashed lines shown in Fig. 6. We then average the absorptance within

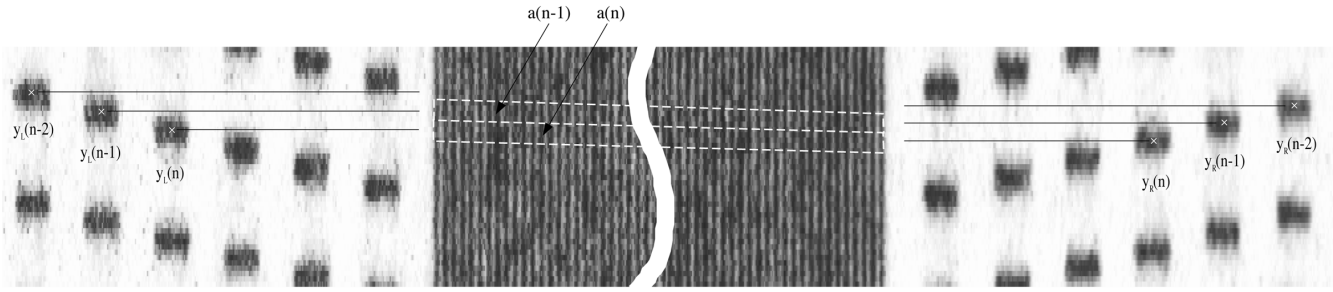

Figure 6. Test pattern scanned at 2000 dpi. For clearer illustration, the image is expanded 4 times in the process direction. The one dimensional absorptance signal $a(n)$ is computed by averaging the image data between the dashed lines. The coordinates of these lines are determined with the help of the corresponding scan line registration marks.

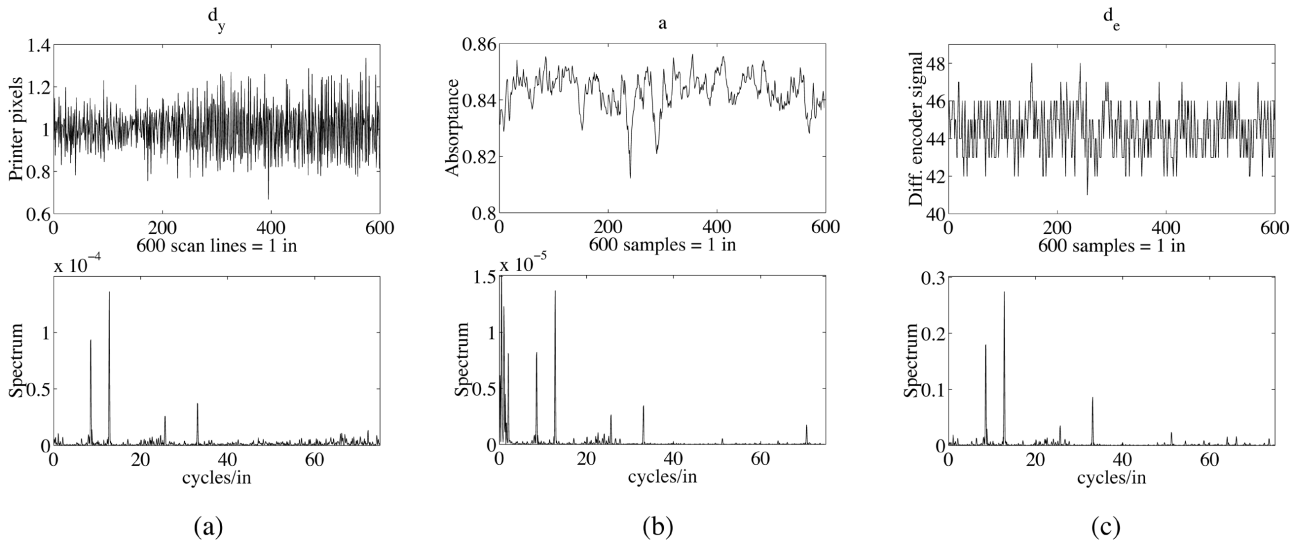

Figure 7. Waveforms and spectra of (a) scan line spacing $d_y(n)$; (b) projected absorptance, $a(n)$; (c) encoder count between scan lines $d_e(n)$. The same major banding frequencies are observed in all three signals.

each cell to obtain the absorptance sequence $a(n)$. We will refer to this as the *projected* absorptance. Note that the cells are skewed due to the fact that the drum continues to rotate as the laser beam scans across it. Figures 7a and 7b show the signal waveforms for the scan line spacing $d_y(n)$ and absorptance $a(n)$. In these figures, we also show the spectra for $d_y(n)$ and $a(n)$. In both spectra, we observe the same main peaks at 8.6, 12.8, 25.6, and 33.1 cycles/in. The absorptance spectrum contains additional very low frequency energy that is not present in the spectrum of the line spacing data. This energy is due to disturbances in the paper path that occur after writing the latent image on the OPC. Conversely, the line spacing spectrum contains high frequency energy not present in the absorptance spectrum. We believe that this energy is due to errors in estimating the centroids of the scan line registration marks.

To establish the relation between scan line spacing $d_y(n)$ and projected absorptance $a(n)$, we format the data as a scatter plot shown in Fig. 8a. From the figure, we see no correlation between $a(n)$ and $d_y(n)$. This is due to the spectral mismatch discussed above. By filtering $a(n)$ and $d_y(n)$ to remove all but the frequency components between 7 and 10 cycles/in (therefore only one spectral peak at 8.6 cycles/in is left), we obtain the scatter plot in Fig. 8b which now shows that $a(n)$ is almost linearly related to $d_y(n)$. The negative slope of this line indicates that as the scan line spacing decreases, the absorptance does indeed increase.

Banding Reduction System

Our basic strategy for banding reduction is to modulate the laser beam exposure time according to the variations in the scan line spacing. In this section, we discuss how laser beam exposure is controlled by pulse width modulation (PWM); and we describe the banding reduction system architecture.

Laser Beam Pulse Width Modulation

To control exposure, one can either adjust the input voltage to the laser beam (amplitude modulation), or adjust the duration of the laser pulses (pulse width modulation or PWM).

Here we use PWM which provides the capability to switch the laser beam on and then off at fractional positions within a nominal printer-addressable pixel. Figure 9 illustrates how different pulse widths p, $0 \le p \le 1$, can be applied with different justifications. In our system, we use only center justification.

In the absence of PWM, the locally averaged absorptance will depend on the bit map sent to the marking engine. For a fixed bit map, the locally averaged absorptance will increase with increasing pulse width p.

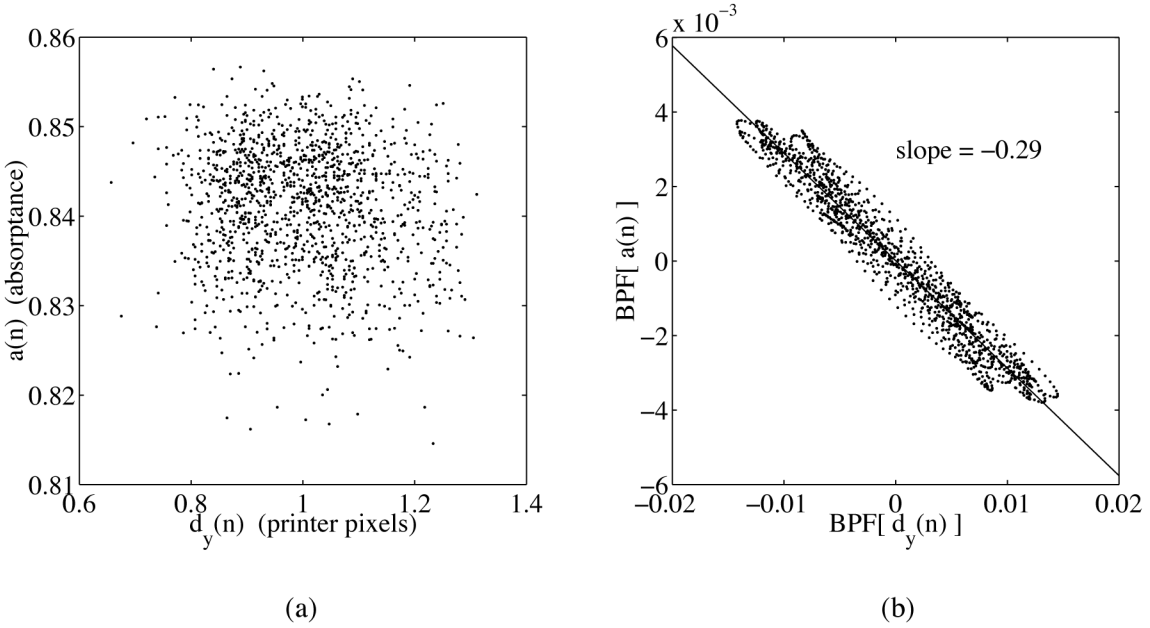

Figure 8. Scatter plot of projected absorptance $a(n)$ versus line spacing $d_y(n)$: (a) signals without filtering; and (b) signals bandpass filtered to [7, 10] cycles/in.

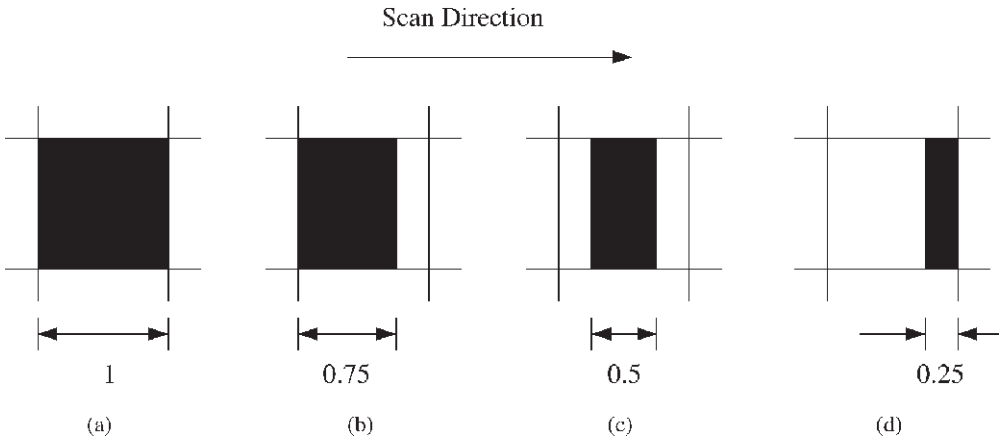

Figure 9. Illustration of pulse width modulation with different justification modes: (a) $p = 1$; (b) $p = 0.75$ with left justification; (c) $p = 0.5$ with center justification; and (d) $p = 0.25$ with right justification.

However, this relationship is generally not linear and may also depend on the bit map itself. In our work, we ignore the dependence on the bit map, and base the banding compensation system on a single relation for average absorptance as a function of pulse width p. We obtain this relation by printing the test page for different fixed values of p, and processing it as described in previous section to obtain absorptance, which in this case, we average over the entire 50% fill region on the page. We will refer to this as the *average* absorptance.

Figure 10 shows the resulting curve for average absorptance $a_0(p)$ as a function of pulse width p. We see that for $0.0 \le p \le 0.3$, there is very little development. Then as p increases from 0.4 to 0.6, the absorptance increases very rapidly to approximately 80% of its maximum value. Beyond $p = 0.7$, the absorptance increases more slowly to its maximum value of 0.84.

While modulating pulse width to compensate banding, we want to operate with as large an average value of p as possible, since this corresponds to the maximum average absorptance that we can print in solid black areas of the page. Thus, we will want to confine our range of operation to $0.7 \le p \le 1.0$. Over this range, the average absorptance can be approximated well as a linear function of pulse width:

$$a_0(p) = \alpha p + \beta, \quad 0.7 \le p \le 1.0, \tag{7}$$

where $\alpha = 0.417$ and $\beta = 0.424$.

System Architecture

Figure 11 shows a block diagram of our banding reduction system. A Canon M1 optical Encoder (Laser Rotary Encoder M1: Canon, Inc., Tokyo, Japan) is mounted on the OPC drum axis. This digital encoder generates 100,000 counts per revolution when operated in double resolution mode. Since the OPC drum circumference is 3.71 in,

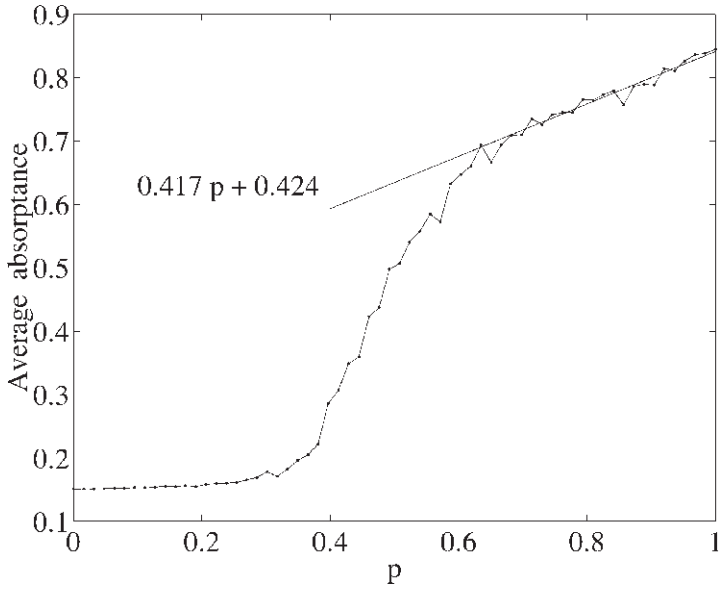

Figure 10. Average absorptance a_0 as a function of pulse width p. For $p \in [0.7, 1]$, we approximate this relation by a linear function as shown.

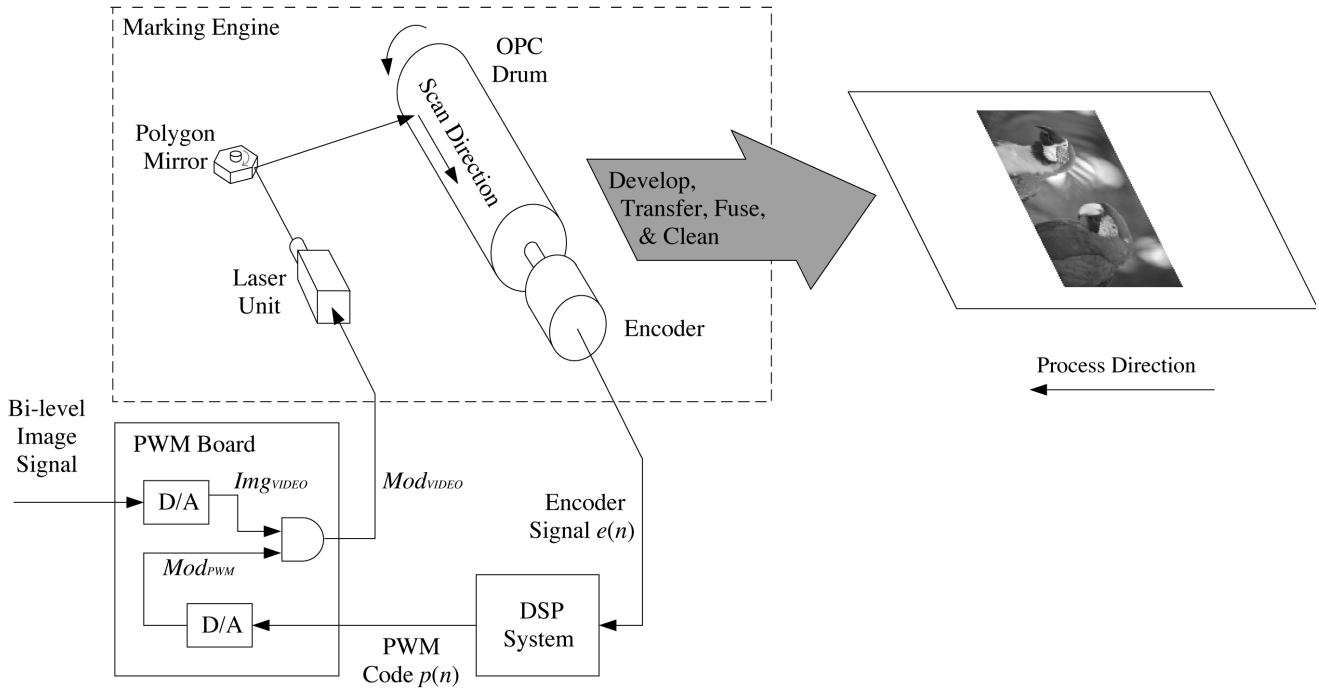

Figure 11. Block diagram of the banding reduction system. An optical encoder is mounted on the OPC drum axis in order to track the speed of the OPC drum. The DSP system computes the PWM code needed for each scan line according to the encoder output. The PWM system modulates the bi-level image signal according to the PWM code.

this corresponds to 44.92 counts per 1/600 inch nominal scan line interval. However, with our experimental setup, the recorded nominal counts are 44.5. This is because the speed of the OPC drive motor is controlled by its own clock signal which may be slightly different from the clock signal that drives the polygon mirror motor.

When the laser beam reaches the left edge of the OPC drum, a beam detect signal is generated. This signal triggers the sampling of the optical encoder output to provide an encoder count for the current scan line. This information is used to generate a pulse width $p(n)$ for the current line, which is kept constant across it. This

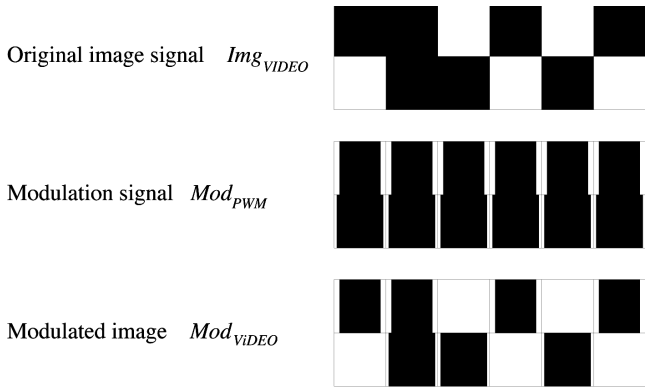

Figure 12. Original halftone image signal, pulse width modulation signal, and resulting modulated image signal. The modulated image is the AND of the original bi-level image signal and the pulse width modulation signal. In the compensation system, we use a fixed pulse width for each scan line.

pulse width must be computed before the laser beam reaches the first addressable pixel on the OPC drum, which is a distance of 0.125 in from the point at which the beam detect signal is generated. Since the laser beam is traveling at a velocity of 9.44×10^3 in/s across the page, we have 13.2 μs to perform this calculation. In our prototype system, the PWM code is computed with a Motorola DSP56002EVM evaluation board (DSP56002EVM: Motorola, Inc., Motorola Literature Distribution, Denver, CO) based on the DSP56002 DSP chip. This chip is a fixed point processor which runs at a clock speed of 80 MHz. At this rate, we can execute 528 instructions to compute the pulse width code, which is an 8 bit value. The most significant 2 bits are used to encode the justification mode; and the least significant 6 bits carry the pulse width information. Here we only use center justification so the most significant 2 bits are set to 0.

The PWM board converts the bi-level digital image signal to an analog video signal Img_{VIDEO}. Running on the same clock, a piggyback board on the PWM board converts the 8 bit PWM code to an analog modulation waveform Mod_{PWM}. The signal Mod_{PWM} is synchronized to Img_{VIDEO} by the laser beam detect pulses, which trigger the DSP system to generate the PWM code line-by-line. Finally, Img_{VIDEO} is AND-ed with Mod_{PWM} as illustrated in Fig. 12, on the piggyback board to generate the modulated video signal Mod_{VIDEO} sent to the laser.

Relation between Encoder Signal and Absorptance Signal

In the section *Test Pattern Analysis*, we printed a specially designed test pattern to determine the relation between line spacing and printed absorptance. In order to develop our compensation algorithm, we need the corresponding relation between encoder count and printed absorptance. We can print the same test pattern as before, and record the encoder count sequence $e(n)$ while the page is being printed. However, we need a way to synchronize the encoder count with the measured absorptance sequence $a(n)$. To do this, we again use the beam detect signal which generates a count that is incremented by one at the start of each line. When the beam detect count reaches a specified value, we initiate sampling of the encoder output and at the same time set the pulse width p equal to 0 for several lines. This generates a clearly identifiable white gap in the test pattern that tells us where to start the sequence $a(n)$ when we analyze the printed test page.

Figure 7c shows the differential encoder signal

$$d_e(n) = e(n) - e(n-1), \tag{8}$$

corresponding to the line spacing and absorptance signals obtained from the printed test pattern. As mentioned earlier, the nominal value for this signal is $d^0_e = 44.5$. Figure 7c also shows the spectrum of this signal. We see that it too contains the same major spectral peaks as the line spacing and absorptance signals. However, it lacks both the low frequency content of the absorptance signal and the high frequency content of the line spacing signal.

To establish the relation between the encoder perturbation

$$\delta_e(n) = d_e(n) - d^0_e, \tag{9}$$

and the projected absorptance perturbation

$$\delta_a(n) = a(n) - a_0, \tag{10}$$

we again use a scatter plot as shown in Fig. 13. By applying a bandpass filter to extract the spectral peak at 8.6 cycles/in, we again see a linear relation between these two signals similar to that shown in Fig. 8b for the absorptance versus line spacing. We can think of the slopes of the lines in Figs. 8b and 13 as a measure of the efficiency of perturbations in line spacing in generating perturbations in absorptance, i.e., banding. When viewed from this perspective and in light of the impact of the nonlinear relation between exposure fluctuations and banding discussed in the section *Banding Artifacts,* and illustrated in Figs. 2 through 4, it is reasonable to expect that the curves in Figs. 8b and 13 will depend on pulse width p, since this determines our operating point along the curve in Fig. 2. Thus we have

$$\delta_a(n, p) = \eta(p)\delta_e(n). \tag{11}$$

By again printing and processing the test pattern for different values of p, we can determine the function $\eta(p)$ which is shown in Fig. 14. We see that the banding efficiency $|\eta(p)|$ decreases with increasing p, over the range of values of p that are of interest, which is what we would expect in view of Fig. 2. In addition, this relation can be modeled well as a linear function of p:

$$\eta(p) = \zeta p + \tau, \quad 0.7 \le p \le 1.0. \tag{12}$$

Here $\zeta = 0.039$ and $\tau = -0.045$ are calculated from Fig. 14 by a least-squares fit to the data.

System Analysis

Compensation Algorithm

Having specified the system architecture and characterized the relation between all of its components in the preceding two sections, we are now ready to derive the compensation algorithm itself. It will specify the desired pulse width p as a function of the differential encoder count d_e to suppress banding. We start by writing the projected absorptance signal as the sum of its nominal value and a perturbation term caused by the OPC drum velocity fluctuations

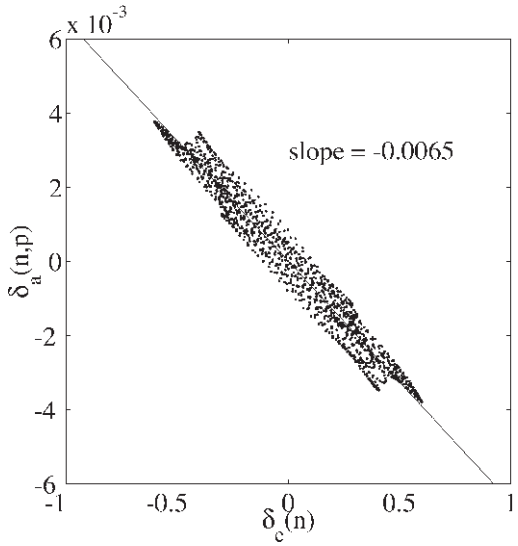

Figure 13. Scatter plot of the absorptance perturbation $\delta_a(n, p)$ versus encoder count perturbation $\delta_e(n)$ with $p = 1$. The perturbation signals are obtained by bandpass filtering to [7, 10] cycles/in.

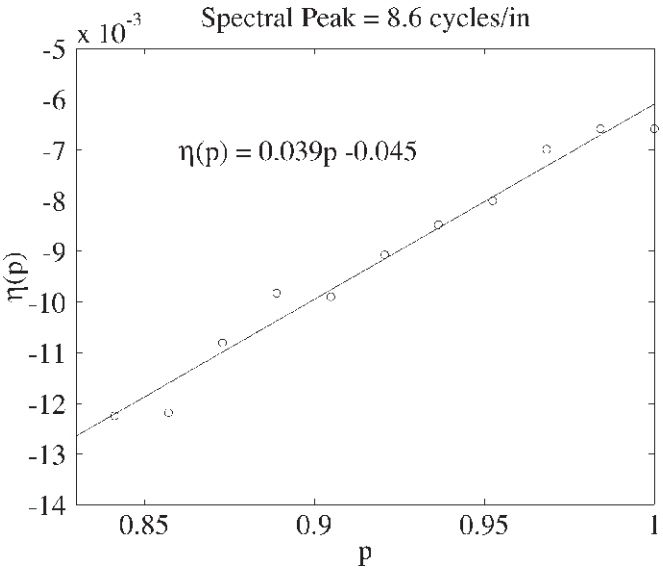

Figure 14. Banding efficiency $\eta(p)$ for the spectral peak at 8.6 cycles/in.

$$a(n) = a_0(p) + \delta_a(n, p). \tag{13}$$

Both these terms depend on pulse width p.

To cancel the perturbation and obtain a fixed $a(n) = a_0(p_0)$, where p_0 is the nominal pulse width, we vary p as a function of n. Therefore, Eq. (13) becomes

$$a_0(p_0) = a_0(p(n)) + \delta_a(n, p(n)). \tag{14}$$

Replacing $a_0(\bullet)$ by the linear model in Eq. (7) and rearranging, we obtain

$$\begin{aligned} \alpha p_0 + \beta &= \alpha p(n) + \beta + \delta_a(n, p(n)), \\ p(n) &= p_0 - \frac{1}{\alpha}\delta_a(n, p(n)). \end{aligned} \tag{15}$$

Next, we replace $\delta_a(n, p(n))$ by Eq. (11) to yield

$$p(n) = p_0 - \frac{1}{\alpha}\eta(p(n))\delta_e(n). \tag{16}$$

Finally, we apply the banding efficiency function from Eq. (12), and rearrange again to obtain

$$\begin{aligned} p(n) &= p_0 - \frac{1}{\alpha}\left(\zeta p(n) + \tau\right)\delta_e(n), \\ p(n) &= \frac{p_0 - \frac{\tau}{\alpha}\delta_e(n)}{1 + \frac{\zeta}{\alpha}\delta_e(n)} = \frac{p_0 - \frac{\tau}{\alpha}(d_e(n) - d_e^0)}{1 + \frac{\zeta}{\alpha}(d_e(n) - d_e^0)}. \end{aligned} \tag{17}$$

As discussed in the *Banding Reduction System* section, we want to choose as large a value of p_0 as possible. From Fig. 7c, we observe that the differential encoder count $d_e(n)$ varies between 41 and 48. The pulse width $p(n)$ will take on its maximum value when $d_e(n)$ is largest, because this is when the scan lines are farthest apart, resulting in the greatest drop in absorptance $a(n)$ in the absence of compensation. Since the pulse width cannot exceed 1, we substitute $p(n) = 1$ and $d_e(n) = 48$ into Eq. (17) and solve for p_0 to obtain $p_0 = 0.941$. With this value of p_0 and $41 \le d_e(n) \le 48$, we will stay within the linear range of $a_0(p)$ for which our model given by Eq. (7) is valid.

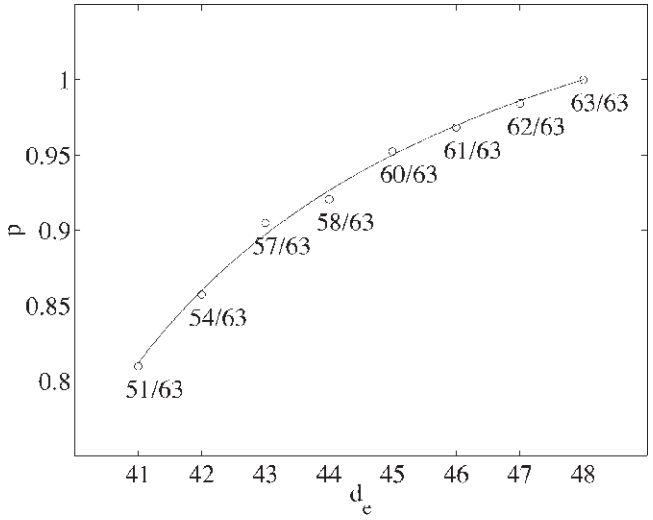

Figure 15. PWM code as a function of differential encoder signal $d_e(n)$.

Figure 15 shows $p(n)$ as a function of the differential encoder signal $d_e(n)$ for this value of p_0. Since our PWM system has only 6 bits for pulse width, $p(n)$ has to be quantized to 64 levels as indicated in Fig. 15 by the sample points. For efficient implementation, we precompute Eq. (17) for the differential encoder counts between 41 and 48, and store these pulse widths as a look-up-table in the DSP system. In the DSP system, the computation of subtracting the previous encoder count from the current count and performing the table look-up can be done in 10 instructions. This is far fewer than the

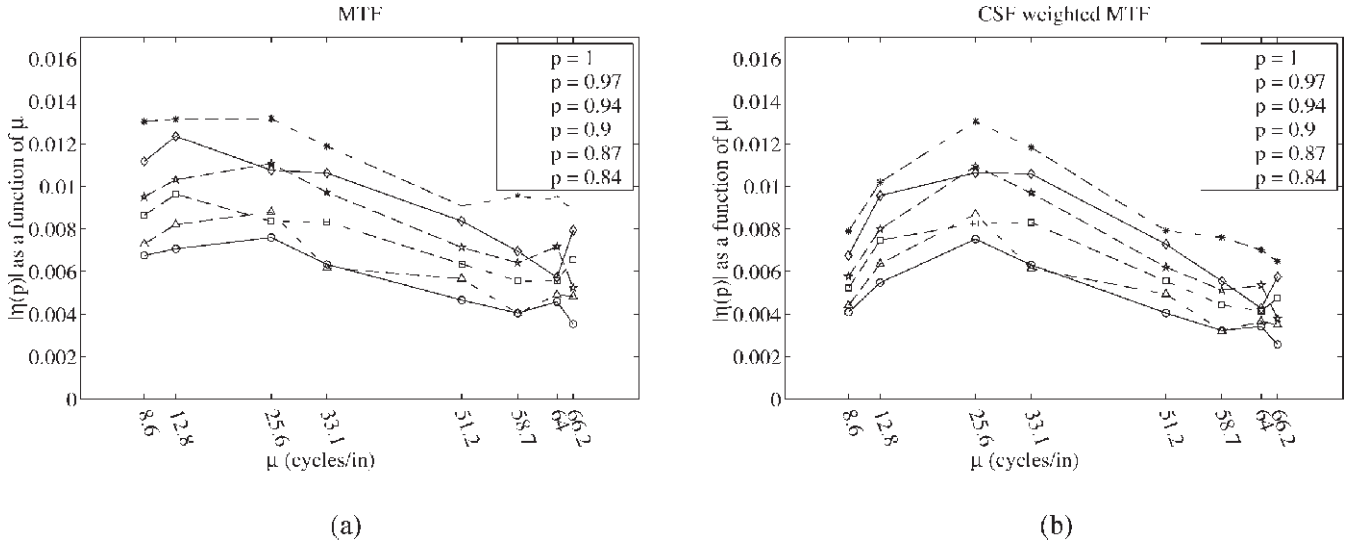

Figure 16. (a) Banding modulation transfer function (MTF); and (b) CSF (viewing distance = 12 in.) weighted MTF.

system constraint of 528 instructions discussed in the *System Architechture* section.

Banding Modulation Transfer Function

In deriving the compensation algorithm given by Eq. (17), we wrote the projected absorptance perturbation $\delta_a(n)$ as the product of the encoder perturbation $\delta_e(n)$ and the banding efficiency $\eta(p)$ (Eq. (11)). We explicitly accounted for the dependence of banding efficiency on pulse width p; but we ignored its dependence on banding frequency μ. In fact, the function $\eta(p)$ shown in Fig. 14 was derived for a single banding frequency of 8.6 cycles/in.

If we fix the pulse width p and think of the overall printer system as one that transforms a sinusoidal fluctuation in line spacing or differential encoder count to a sinusoidal fluctuation in absorptance, then the banding efficiency η in Eq. (11) is the frequency response of this system. If we plot it as a function of spatial frequency, we obtain the modulation transfer function (MTF) for banding shown in Fig. 16a. This function was obtained by measuring the slope of scatter plots like that shown in Fig. 13 for each banding frequency observed in Fig. 7c with pulse width $p = 1$. For each such frequency, these scatter plots are based on data obtained by filtering both $\delta_a(n)$ and $\delta_e(n)$ with a narrowband filter centered at that frequency.

In Fig. 16b, we include the effect of the human viewer by cascading the contrast sensitivity function[18] with the banding MTF. Figure 16a shows that the banding MTF is fairly flat out to a spatial frequency of 30 cycles/in. On the other hand, Fig. 16b shows that the overall system, including the human viewer with viewing distance 12 in, is most efficient in transforming fluctuations in line spacing to visible banding at around 30 cycles/in.

So far in our discussion of the frequency dependence of banding, we have kept the pulse width p constant. To reduce banding, we of course want to vary p; so we need to consider how banding efficiency depends on p at each fixed spatial frequency μ. What we find is that at each such frequency the model given by Eq. (12) holds well with the values for slope ζ and intercept τ given in Table I. Examining Table I, we see that the variation in the parameters ζ and τ is relatively small (less than 5% for both of them) over the range of frequencies [8.6–33.1] cycles/in within which there is significant energy in the line spacing perturbations (Fig. 7c), and which will yield highly visible fluctuations in absorptance (Fig. 7b). Thus, in the interest of simplicity, we use a single set of values for ζ and τ. Since the peak energy in Fig. 7c occurs at 12.8 cycles/in, we choose $\zeta = 0.040$ and $\tau = -0.047$, corresponding to the measurements made at 12.8 cycles/in.

TABLE I. Parameters for the Model of the Relationship between the Magnitude of the Absorptance Signal and the Magnitude of the Encoder Count Signal Given by Eq. (12).

μ (cycles/in)	ζ	τ
8.6	0.039	–0.045
12.8	0.040	–0.047
25.6	0.036	–0.043
33.1	0.038	–0.044
51.2	0.024	–0.029
58.7	0.030	–0.034
64.0	0.024	–0.028
66.2	0.027	–0.031

Experimental Results

Figure 17 shows the test pattern and a halftone image printed without banding reduction. The halftone parrot image is generated using the direct binary search (DBS) algorithm.[19] Figure 18 shows same images printed with banding reduction. Comparing them, we see that the banding artifacts are significantly reduced. Figure 19 shows the spectra of the projected absorptance of the 50% fill pattern without and with banding reduction. To better illustrate the visual significance of these results, we also show the spectra weighted by the contrast sensitivity function[18] of the human viewer. We observe that the main spatial frequency peaks are suppressed after banding reduction. However, we still see the low frequency components and also a peak at 70 cycles/in. Those frequency components are induced outside of the OPC drum and cannot be detected by the encoder. To suppress them, we would need to have other sensors to acquire the information from the perturbation sources.

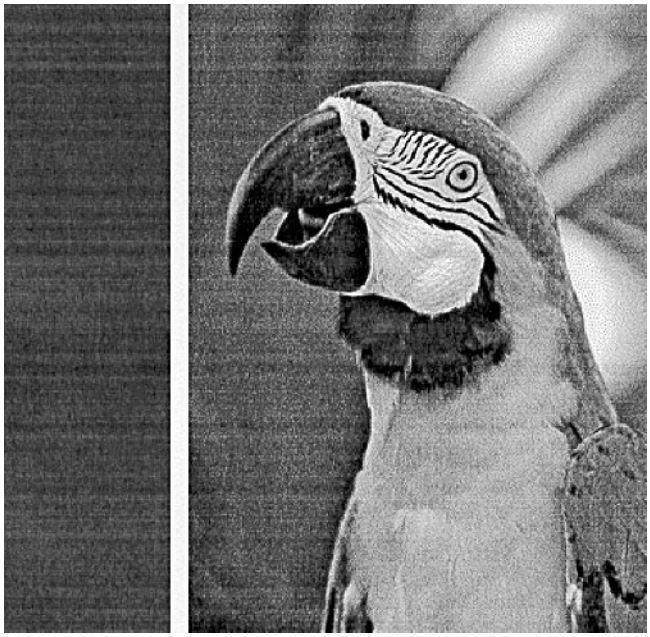

Figure 17. Test pattern (left) and a halftone image (right) without banding reduction.

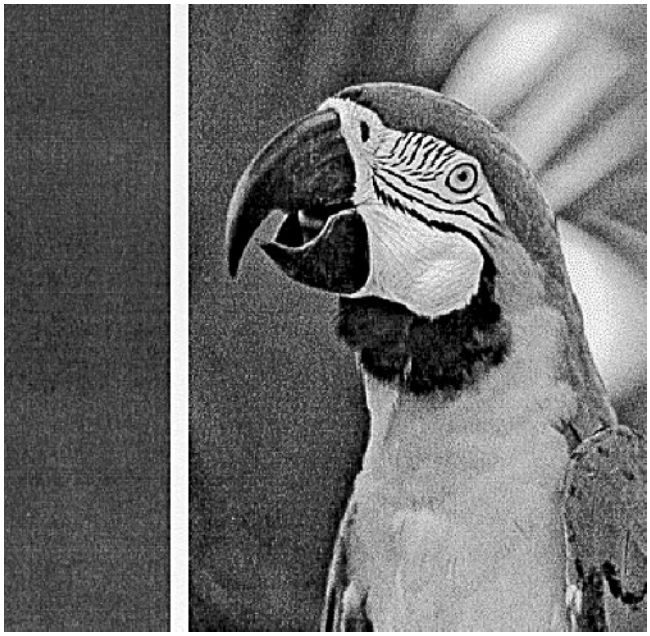

Figure 18. Test pattern (left) and a halftone image (right) with banding reduction.

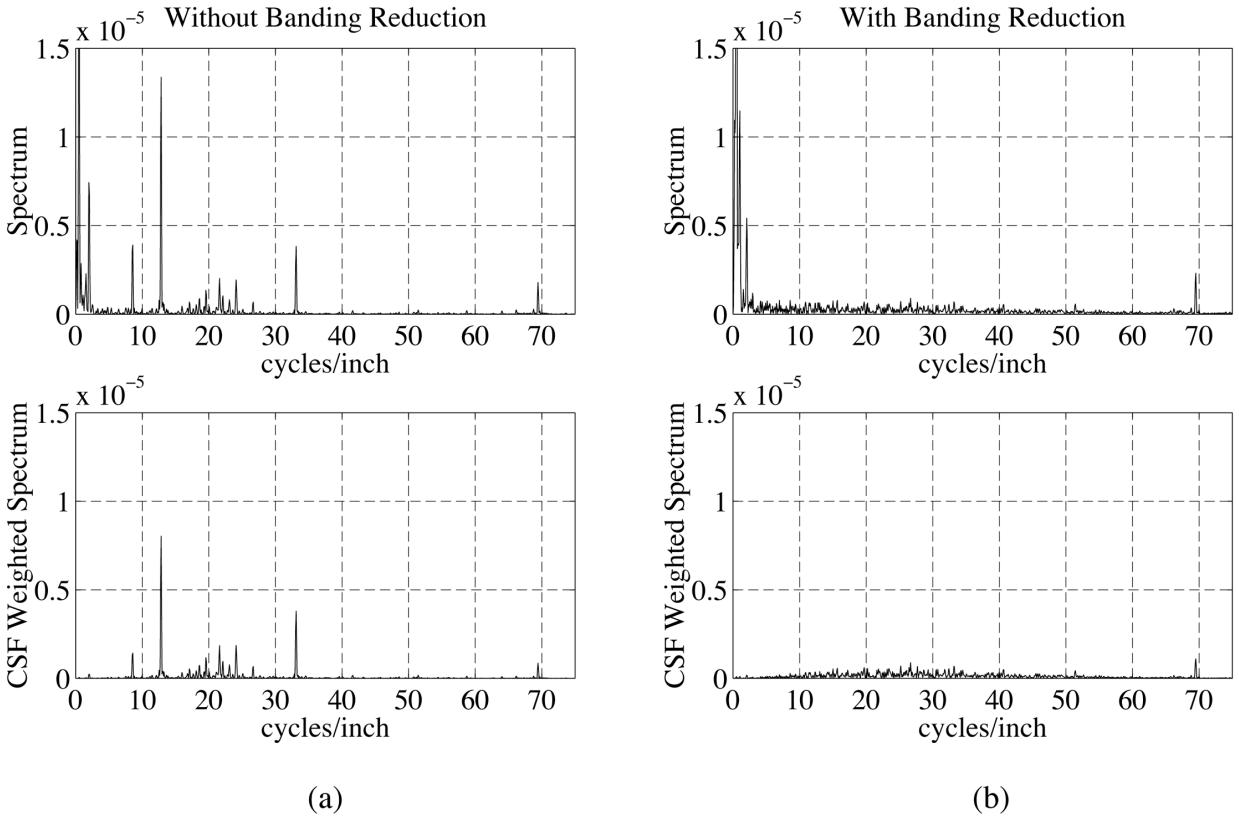

Figure 19. Spectra unweighted (top row) and weighted by the contrast sensitivity function[18] (bottom row) for the human viewer (12 in. viewing distance) (a) without, and (b) with banding reduction. In (b), the low frequencies and the peak at 70 cycles/in are not compensated because the encoder cannot detect those banding sources.

Conclusion

Banding is an important artifact for EP printers. It is primarily caused by fluctuations in the OPC drum velocity. These fluctuations result in variations in line spacing, causing excessive development if the line spacing is too small, and too little development if the line spacing is too large. We have proposed a system for reducing banding that is based on sensing the OPC drum velocity fluctuations with an optical encoder mounted on the drum shaft. We then modulate the laser beam pulse width line-by-line to compensate for the impact of line-spacing errors on development.

We have implemented a prototype system using an HP LaserJet 4M 600 dpi printer. We characterized the system by printing a special test page using a fixed pulse width, while simultaneously recording the optical encoder output. We then scanned the page, and analyzed it to extract information about fluctuations in line spacing and absorptance. We repeated this process for all pulse widths between 0 and 1. From these measurements, we found that average absorptance increases linearly with pulse width over the range of pulse widths of interest, and that perturbations in projected absorptance are negatively proportional to perturbations in the encoder count. Since the banding modulation transfer function is nearly flat over the range of frequencies at which significant visible banding is caused by OPC drum velocity fluctuations, we ignored frequency dependence in the design of the compensation algorithm.

Our experimental results show that the method suppresses very well the banding due to fluctuations in OPC drum velocity. However, lower frequency banding due to other sources in the printer is not suppressed. Suppression of banding at these frequencies would require additional sensors to capture the sources of the low frequency fluctuation. Although we have not demonstrated it in this system, we believe that our compensation algorithm can be modified for use in a system in which it is desired to exploit pulse width modulation both as part of the halftoning algorithm and to suppress banding. ⚠

Acknowledgment. We gratefully acknowledge the support from the Hewlett Packard Company. We also acknowledge Farhan Baqai's contribution to the design of the test pattern.

References

1. P. Burns, M. Rabbani and L. Ray, Analysis of Image Noise Due to Position Errors in Laser Writers, *Applied Optics* **25,** 2158–68 (1986).
2. P. Melnychuk and R. Shaw, Fourier Spectra of Digital Halftone Images Containing Dot-Position Errors, *J. Opt. Soc. Amer.* **5,** 1328–38 (1988).
3. D. Haas, Contrast Modulation in Halftone Images Produced By Vibration in Scanline Spacing, *J. Imaging Technol.* **15,** 48–55 (1989).
4. R. Loce, W. Lama and M. Maltz, Modeling Vibration-Induced Halftone Banding in a Xerographic Laser Printer, *J. Electronic Imaging* **4,** 8–61 (1995).
5. P. Jeran, Gear Train Control System for Reducing Velocity Induced Image Defects in Printers and Copiers, US Patent 5,812,183 (1998).
6. H. Kawamoto, K. Udagawa and M. Mori, Vibration and Noise Induced by Electrostatic Force on a Contact Charger Roller of Electrophotography, *J. Imaging Sci. Technol.* **39,** 477–480 (1995).
7. H. Kawamoto, Chatter Vibration of a Cleaner Blade in Electrophotography, *J. Imaging Sci. Technol.* **40,** 8–13 (1996).
8. W. Foote and R. Sevier, Laser Printer with Apparatus to Reduce Banding by Servo Adjustment of a Scanned Laser Beam, US Patent 5,760,817 (1998).
9. R. Lawton and D. Marshall, Beam Deflecting for Resolution Enhancement and Banding Reduction in a Laser Printer, US Patent 5,920,336 (1999).
10. W. Lama, R. Loce and J. Durbin, Image Bar Printer Compensated for Vibration-Generated Scan Line Errors, US Patent 4,801,978 (1989).
11. R. Loce and W. Lama, Halftone Banding Due to Vibrations in a Xerographic Image Bar Printer, *J. Imaging Technol.* **16**, 6–11 (1990).
12. R. Morrison, System and Method for Modifying an Output Image Signal to Compensate for Drum Velocity Variations in a Laser Printer, US Patent 5,729,277 (1998).
13. D. Costanza, R. Jodoin and R. Loce, Method and Apparatus for Compensating for Raster Position Errors in Output Scanners, US Patent 5,900,901 (1999).
14. E. M. Williams, *The Physics and Technology of Xerographic Processes*. John Wiley and Sons, New York, NY, 1984.
15. D. E. Bugner, A review of electrographic printing, *J. Imaging Sci.* **35,** 6, 377–386 (1991).
16. L. B. Schein, *Electrophotography and Development Physics*. Morgan Hill, CA: Laplacian Press, 2 ed., 1996.
17. D. Kacker, T. Camis and J. P. Allebach, Electrophotographic Process Embedded in Direct Binary Search, *IEEE Trans. on Image Processing*, **11,** 234-257 (2002).
18. F. W. Campbell and D. G. Green, Optical and retinal factors affecting visual resolution, *J. Physiology* **181,** 576–593 (1965).
19. D. J. Lieberman and J. P. Allebach, A Dual Interpretation for Direct Binary Search and its Implications for Tone Reproduction and Texture Quality, *IEEE Trans. on Image Processing*, **9,** 1950-1963, (2000).